Ferritin Protein Nanocages for Selective Separation and Recovery of Critical Metals

Zhiqian Han[a], Yifei Ma[a], Meng Wang[a,*]

[a]Department of Civil and Environmental Engineering, University of Pittsburgh, 3700 O'Hara St., Pittsburgh, PA 15261

*Address correspondence to meng.wang@pitt.edu, 412-624-9207

ABSTRACT

Recycling critical metals from waste streams is increasingly important to meet the rising demand for clean energy technologies and reduce the environmental impact of ore mining. A key step in this process is the selective separation and recovery of high-grade metals from waste leachates containing complex metal mixtures; however, current strategies are limited by high chemical, energy, and resource consumption, substantial financial costs, and production of hazardous byproducts. Herein, we report the pioneering use of ferritin – self-assembling protein nanocages with porous, hollow structures and supercharged inner surfaces – as a high-efficiency biosorbent for eco-friendly, selective metal recovery from mixtures. Ferritin nanocages adsorbed cobalt (Co^{2+}), nickel (Ni^{2+}), and lithium (Li^{+}) primarily through electrostatic interactions, localizing the adsorbed metal cations within their cavities. Adsorption isotherms indicated significantly more effective adsorption of Co^{2+} and Ni^{2+} compared to Li^{+}, enabling efficient Co^{2+}/Ni^{2+} separation from Li^{+}. Leveraging ferritin's ability to concentrate adsorbed metal cations within cavities enabled selective recovery of Co^{2+} as nearly 95% pure solid carbonate salts from Co^{2+}-Li^{+} mixtures through single-step precipitation under mild conditions, while Li^{+} remained in solution. This research opens new avenues for using ferritin nanocages in selective metal separation and recovery from waste streams via simple, environmentally benign adsorption-precipitation processes.

KEYWORDS

biosorption, biometallurgy, waste stream, protein shell, pore, precipitation.

SYNOPSIS

This research pioneered the use of ferritin protein nanocages for eco-friendly, selective metal separation and recovery from mixtures through simple adsorption-precipitation processes.

29 **TABLE OF CONTENTS**

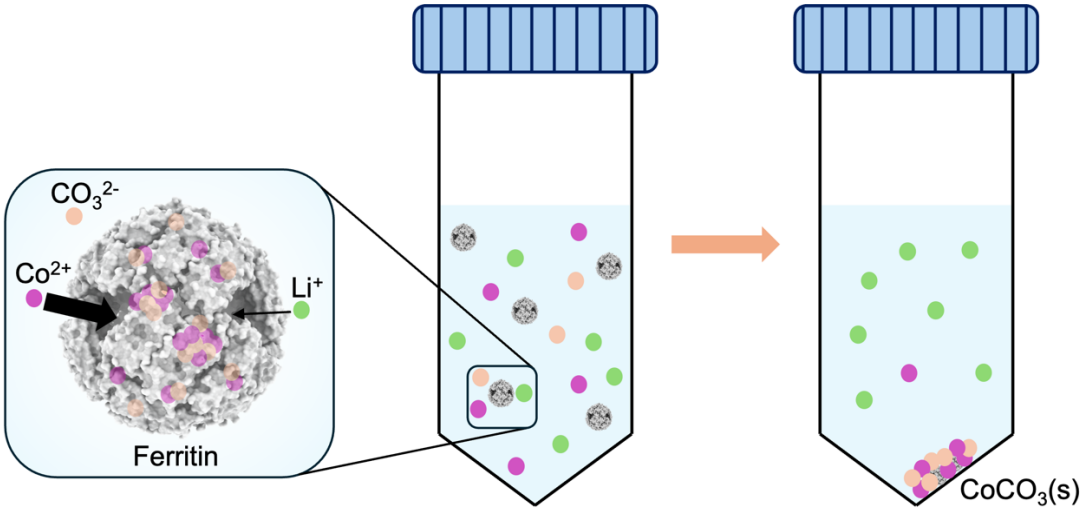

30

INTRODUCTION

The ongoing shift toward a low-carbon society is driving an ever-increasing demand for critical metals such as cobalt, nickel, lithium, and rare earth elements (REEs), which are crucial components in clean energy technologies.[1] Traditionally, mining ores has been the primary method for obtaining these metals, yet this process carries significant environmental burdens.[2,3] To address this growing demand, there is a rising interest in recycling metals from waste, particularly electronic waste (E-waste), as a sustainable alternative to ore mining.[4,5] E-waste is among the fastest-growing waste streams globally and contains diverse critical metals, even at concentrations higher than those found in high-grade ores.[6] A key step in metal recycling is the separation and recovery of leached metal ions, where these ions are selectively isolated from mixed solutions and subsequently recovered as solid materials that can be reused in manufacturing processes.[7,8] Current practices for metal separation and recovery largely depend on physicochemical methods, such as solvent extraction and electrodeposition, which, although effective, are resource-intensive, require substantial amounts of chemicals, energy, and financial inputs, and generate hazardous waste.[9,10]

In this regard, biometallurgy, an approach that leverages biosorption and biocatalysis to separate and recover metals, offers a range of advantages of reduced energy consumption, lower chemical usage, and minimal environmental impact, positioning it as a promising substitute for the physicochemical methods.[9,11–13] For instance, the protein lanmodulin (LanM) exhibits strong binding affinities for REE ions, with a 1:2-3 stoichiometry, even in the presence of competing elements.[14–17] This high selectivity has enabled the successful application of LanM in recovering REEs from various sources, such as E-waste leachate, lignite leachate, and geothermal brine, under ambient conditions and without the need for organic solvents typically required in conventional solvent extraction-based REE separation.[18,19]

Ferritin is a protein that self-assembles into highly organized, hollow, spherical nanocages with a diameter of approximately 10 nm.[20] These nanocages comprise a porous protein shell formed by 24 identical ferritin protein subunits and are ubiquitously used by organisms to sequester and store iron in their interior cavity (Figure 1A).[19,21,22] Beyond iron, previous in vitro studies have shown that ferritin nanocages can also

take up other metal ions.[23,24] However, there has been limited investigation into ferritin's potential for selective metal recovery from mixture solutions. Unlike LanM, which binds to REE ions at four specific sites on the protein,[14] the ferritin nanocage features an inner surface rich in acidic amino acid residues, creating a dense cluster of negative charges that enables it to take up and sequester metal cations in the cavity through electrostatic interactions.[25] The nanocage's open pores play a crucial role in determining its affinity for different metal cations by controlling their influx and efflux.[19,22] These unique capabilities allow ferritin nanocages to bind metal cations at a much higher capacity and concentrate them within the cavity, which could be potentially leveraged to facilitate metal ion recovery.

The objective of this study is to explore the use of ferritin nanocages to selectively separate and recover metals from a synthetic mixture containing Co^{2+}, Ni^{2+}, and Li^{+}, which are chosen for their co-existence in lithium-ion batteries.[26] We investigate the adsorption isotherms of these three metal ions within ferritin nanocages and assess the nanocage's ability to separate them one from another. To further enhance metal recovery, we examine the feasibility of combining the nanocage's metal ion concentration capability with precipitation reactions, aiming to integrate both separation and recovery into a single, streamlined process. Through this approach, we seek to establish a proof of concept for using ferritin nanocages as a sustainable solution for metal recovery from mixed-metal systems.

MATERIALS AND METHODS

Materials

All chemicals and biological reagents used in this study are listed in the Supporting Information (SI).

Ferritin Synthesis, Purification and Characterization

Ferritin from *Archaeoglobus fulgidus* (AfFtn) was selected as the model ferritin for this study.[22] It was expressed in *Escherichia coli*, purified through size-exclusion chromatography (SEC), and characterized using sodium dodecyl sulfate-polyacrylamide gel electrophoresis (SDS-PAGE), dynamic

light scattering (DLS), and negative-stain transmission electron microscopy (TEM). Details are provided in the SI.

Metal Ion Separation and Recovery

The evaluation of metal ion adsorption and separation by AfFtn nanocages and selective Co^{2+} recovery through AfFtn-facilitated precipitation are described in detail in the SI.

RESULT AND DISCUSSION

AfFtn Synthesis, Purification, and Characterization

The successful synthesis of AfFtn was confirmed by SDS-PAGE, which showed a prominent protein band around 20 kDa, consistent with its predicted size based on the amino acid sequence (Figure S1A).[19,22] Following heat treatment and salt precipitation, most of the contaminant cellular proteins were removed. Further purification was achieved using SEC, where the majority of AfFtn eluted at 0.8 column volume (CV) (Figure S1B&C), agreeing with the assembled, intact AfFtn nanocages, as reported in previous work.[22] Peaks containing AfFtn, eluting after the major 0.8 CV peak, correspond to either partially assembled nanocage or AfFtn monomers, likely due to incomplete assembly of the protein.[19] To further verify the integrity of AfFtn nanocages from the 0.8 CV peak, DLS and TEM were performed. DLS analysis revealed a hydrodynamic diameter of approximately 10.7 nm (Figure 1B), closely matching the size of assembled AfFtn nanocages, and TEM images (Figure 1C & Figure S2) further confirmed that the nanocages showed intact assembly with well-defined spherical morphology.[19,22,27]

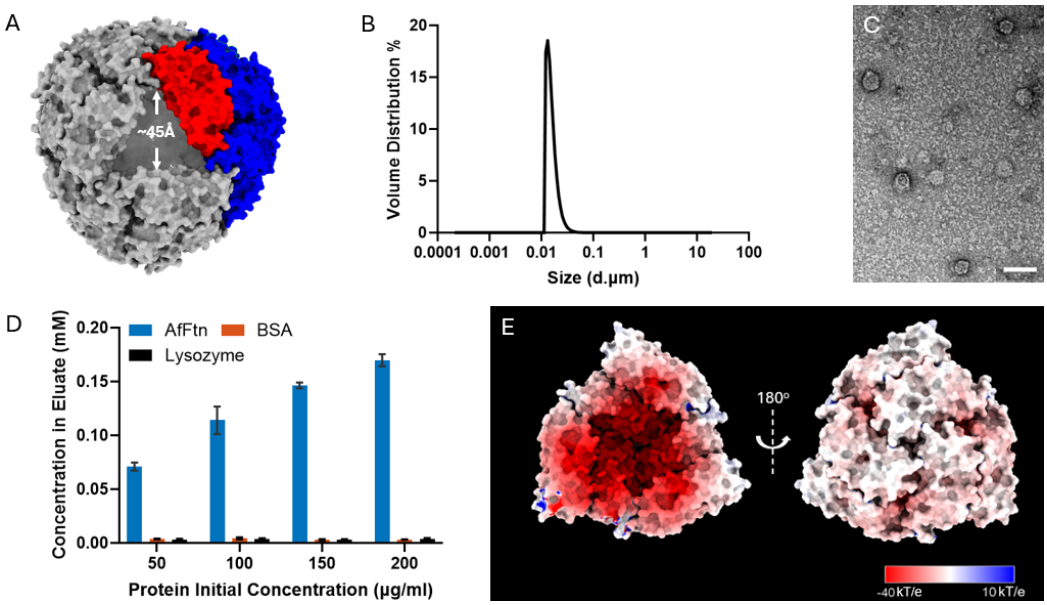

Figure 1. Characterization of AfFtn ferritin nanocages. (A) Structural illustration of an assembled ferritin nanocage (AfFtn, PDB: 1SQ3) with a hexamer colored in blue and a monomer in red. It has four open pores measuring 45 Å. (B) DLS analysis of purified AfFtn nanocages showed a hydrodynamic diameter of approximately 10.7 nm. (C) Negative-stain TEM image of purified AfFtn nanocages, exhibiting spherical morphologies with "dark" stained edges. Scale bar: 50 nm. (D) Concentration of Co^{2+} in the desalting column eluate, indicating strong adsorption of Co^{2+} by AfFtn nanocages, in contrast to negligible adsorption by BSA and lysozyme. Error bars represent the standard deviation of three replicates. (E) Electrostatic surface potential of an AfFtn hexamer, highlighting the clustered negative charge of the inner surface (left) compared to the exterior (right) surface of the nanocage. The potential was calculated at pH 8.0 using PDB2PQR and Adaptive Poisson-Boltzmann Solver (APBS),[28] and visualized with ChimeraX.[29–31]

Metal Ion Adsorption by AfFtn Nanocages

The ability of AfFtn nanocages to adsorb metal cations was first evaluated using Co^{2+} ions by simply mixing them with purified AfFtn nanocages. After overnight incubation, free and AfFtn-adsorbed Co^{2+} were separated by passing the mixture through a desalting column packed with SEC gels. The gels captured free metal ions while allowing the AfFtn nanocage-adsorbed metal ions to remain in the column eluate, which was subsequently analyzed using Inductively Coupled Plasma-Optical Emission Spectrometry (ICP-OES). As shown in Figure 1D, a significant amount of Co^{2+} was detected in the eluate when AfFtn was present, with concentrations increasing proportionally to AfFtn levels. In contrast, negligible amounts of Co^{2+} were observed in the desalting column eluate when control proteins, lysozyme and bovine serum albumin (BSA), were used, indicating minimal Co^{2+} adsorption by these proteins. This outcome was expected for lysozyme, as it carries a positive net charge of approximately +5.2 at pH 8 (Figure

S3), leading to electrostatic repulsion between the protein and Co^{2+} ions. On the other hand, BSA, although carrying a similar negative charge to the AfFtn protein (Figure S3), still exhibited negligible Co^{2+} in the eluate. This significant difference suggests the critical role of AfFtn's assembly in enhancing its adsorption affinity for metal cations. As illustrated in Figure 1E, the assembled AfFtn nanocage displays a highly concentrated cluster of negative charges on its inner surface, which could result in stronger electrostatic interactions that foster efficient adsorption of complementarily charged Co^{2+} ions.[32,33]

We then assessed the adsorption isotherms of Co^{2+}, Ni^{2+}, and Li^{+} by AfFtn to determine whether the nanocages exhibit selectivity for different metal ions. Figure 2A shows that Co^{2+} and Ni^{2+} were adsorbed significantly more effectively by AfFtn than Li^{+}, with all three ions fitting well to the Langmuir isotherm. Li^{+} exhibited the lowest adsorption capacity (Q_m) at 0.250 mmol/g AfFtn protein with a Langmuir equilibrium constant (K_L) of 2.81 mM^{-1}. In contrast, Ni^{2+} had a Q_m of 4.66 mmol/g protein and a K_L of 2.27 mM^{-1}, while Co^{2+} displayed the highest adsorption capacity, with a Q_m of 14.5 mmol/g protein and a K_L of 0.349 mM^{-1}. Based on the molecular weight of AfFtn, each nanocage has the capacity to adsorb around 123 Li^{+}, 7162 Co^{2+}, and 2295 Ni^{2+} ions (see Text S3 in SI). Notably, the adsorption of Co^{2+} and Ni^{2+} reached equilibrium rapidly within minutes (Figure 2B), a trend also observed in the adsorption of REEs onto LanM proteins.[18]

Metal cation adsorption by ferritin can occur on either the nanocage's outer or inner surface.[25] Outer surface adsorption primarily relies on forming coordination bonds at a limited number of specific binding sites, while inner surface adsorption is largely driven by electrostatic attraction between the negatively charged inner surface and the cations. This distinction results in significant differences in adsorption stoichiometry: outer surface adsorption accommodates tens of metal cations per nanocage, whereas inner surface adsorption can host hundreds to thousands of metal cations.[25] Therefore, given the adsorption capacities observed for Li^{+}, Co^{2+}, and Ni^{2+}, we reason that these three metal cations are predominantly adsorbed through electrostatic interactions with AfFtn's inner surface, localizing within the nanocage's cavity. This explains the lower adsorption efficiency of Li^{+}, as it carries only a single positive charge (+1). Regarding Co^{2+} and Ni^{2+}, although both have +2 charges, they exhibit notable differences in Q_m and K_L

values. The transport of ions in and out of assembled AfFtn nanocages occur through the open pores between hexamers (Figure 1A), which are approximately 4.5 nm, much larger than the size of metal cations,[27] suggesting that size exclusion by the pores is unlikely to account for the observed difference in Co^{2+} and Ni^{2+} adsorption. Instead, it is likely that additional factors, such as interactions between the side chains of specific amino acids lining these pores,[19,25] may influence the passage and eventual adsorption of metal cations. As Co^{2+} and Ni^{2+} cations traverse the pores, they may encounter varying degrees of affinity depending on the chemical structure of these side chains, potentially contributing to the differences in their adsorption parameters. Further investigation into these interactions is required to fully understand their exact roles.

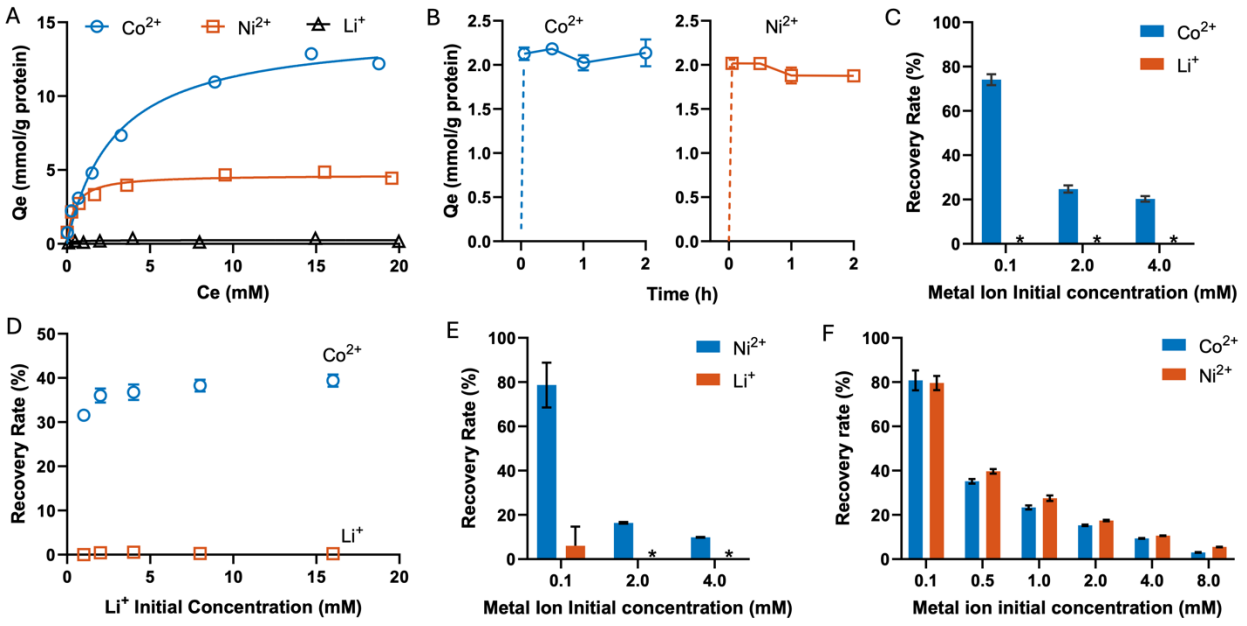

Figure 2. Metal ion adsorption by AfFtn nanocages. (A) Adsorption isotherm for Co^{2+}, Ni^{2+}, and Li^{+}. (B) Adsorption kinetics for Co^{2+} and Ni^{2+}. (C) Recovery rates of Co^{2+} and Li^{+} from mixtures of equal concentrations in the desalting column eluate, suggesting the selective adsorption of AfFtn nanocages for Co^{2+} over Li^{+}. * indicates that concentrations in the eluate were below the detection limit. (D) Recovery rates of Co^{2+} in the presence of varying concentrations of Li^{+}. (E) Recovery rates of Ni^{2+} and Li^{+} from their equal concentration mixtures. * indicates that concentrations in the eluate were below the detection limit. (F) Recovery rates of Co^{2+} and Ni^{2+} from mixtures of equal concentrations, suggesting limited separation between these two ions. All error bars represent the standard deviation of three replicates.

Metal Ion Separation through AfFtn Adsorption

Based on the differential adsorption isotherms of Li^+, Co^{2+}, and Ni^{2+}, we next evaluated AfFtn nanocages for selectively separating metal ions from mixtures. Equal concentrations of Li^+ and Co^{2+} were mixed with AfFtn nanocages, incubated overnight, and then passed through desalting columns, and metal ion concentrations in the eluate were analyzed to determine the recovery rate for each species. As shown in Figure 2C, at an initial concentration of 100 μM, the recovery rate of Co^{2+} in the eluate reached nearly 80%, while Li^+ recovery was negligible (< 1%). This suggests that the eluate contained predominantly Co^{2+} ions, demonstrating that AfFtn nanocages selectively adsorbed Co^{2+} from the Li^+ and Co^{2+} mixture, which enabled effective separation of the two ions. As the initial metal ion concentration increased, the recovery rate of Li^+ remained at a consistently low level, while Co^{2+} recovery decreased, likely due to the AfFtn nanocages reaching their adsorption capacity. It was also found that Li^+ concentration in the initial mixture had minimal impact on the recovery rate of Co^{2+}. At a Co^{2+} initial concentration of 1 mM, increasing the Li^+ concentration did not significantly alter the recovery rate of Co^{2+} in the eluate (Figure 2D), further confirming the preferential adsorption of Co^{2+} over Li^+ by AfFtn nanocages. Similar results were also observed for the Li^+ and Ni^{2+} mixture, where Ni^{2+} dominated in the desalting column eluate (Figure 2E). Furthermore, although Co^{2+} and Ni^{2+} showed different adsorption isotherm parameters for AfFtn nanocages, the separation between these two ions was limited, as indicated by their similar recovery levels in the eluate (Figure 2F). A slightly higher recovery rate of Ni^{2+} was observed at initial concentrations exceeding 0.5 mM, possibly due to the stronger affinity of Ni^{2+} (as suggested by its larger K_L value) to AfFtn nanocages.

Selective Co^{2+} Recovery through AfFtn-Facilitated Precipitation

As discussed above, each AfFtn nanocage has the capacity to adsorb around 7000 Co^{2+} ions, primarily through electrostatic interactions with its negatively charged inner surface, locating these ions within the nanocage cavity. Assuming a uniform spatial distribution of Co^{2+} ions inside the cavity, we estimate that the local concentration of Co^{2+} within the nanocage is equivalent to ~43 M (see Text S3 in SI), which is hundreds of times higher than the bulk solution concentration. This highly concentrated Co^{2+} in AfFtn nanocages presents an opportunity for direct, selective recovery of Co^{2+} from mixtures as solids via

simple precipitation reactions. To test this, we mixed an equal concentration of Co^{2+} and Li^{+} in an AfFtn solution and added sodium bicarbonate to provide CO_3^{2-} ions for Co^{2+} precipitation. The mixture pH was buffered at 8.0. After overnight incubation and centrifugation, a purplish pellet formed at the bottom of the tube, and the pellet size increased over time (Figure 3A). X-ray diffraction (XRD) analysis of the pellet showed peaks matching the characteristic pattern of cobalt carbonate (Figure S4), suggesting its formation through precipitation reactions between Co^{2+} and CO_3^{2-}. In contrast, without AfFtn nanocages, no visible precipitation was observed even after five days of incubation, highlighting the critical role of AfFtn in facilitating Co^{2+} precipitation. Additionally, no precipitation occurred in the absence of $NaHCO_3$.

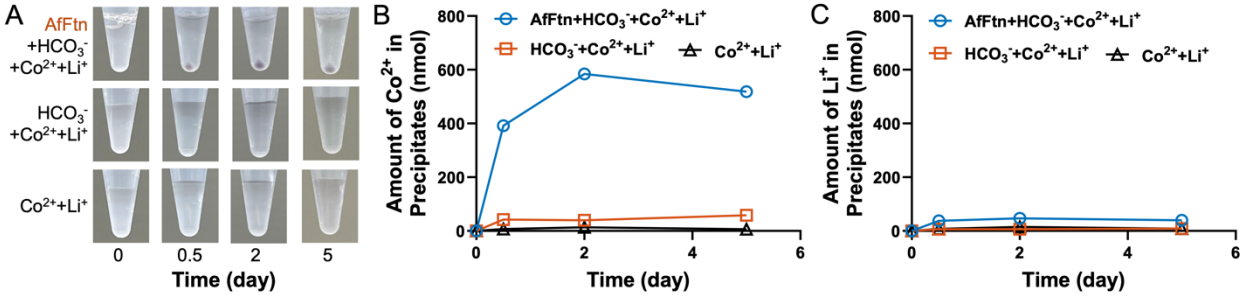

Figure 3. AfFtn nanocage-facilitated selective precipitation of Co^{2+}. (A) Images of precipitation reaction solutions under various conditions after centrifugation. Significant purplish pellets were only observed in reactions containing AfFtn nanocages. (B) Co^{2+} recovered in pellets after centrifugation. (C) Li^{+} recovered in pellets after centrifugation. All error bars represent the standard deviation of three replicates. Some error bars are not visible as they are smaller than the symbol.

In parallel experiments, after removing the supernatant following centrifugation, any remaining visible or invisible pellets were dissolved in diluted nitric acid and subjected to ICP-OES analysis to quantify the amount of Co^{2+} and Li^{+} in the precipitates. Figure 3B shows that, in the presence of both AfFtn and $NaHCO_3$, the amount of Co^{2+} in the precipitates rapidly increased within the first two days, reaching 585 nmol. In comparison, without AfFtn, only 39 nmol Co^{2+} was recovered in the precipitates after five days of incubation, 15 times lower than with AfFtn. When $NaHCO_3$ was absent, Co^{2+} precipitation was nearly zero. More notably, Li^{+} was negligible in the precipitates across all experimental conditions (Figure 3C). As AfFtn nanocages selectively adsorb Co^{2+} ions, they create locally concentrated hotspots of Co^{2+} within their cavities, facilitating the precipitation of Co^{2+} with CO_3^{2-} ions. This selective precipitation allows

for the direct separation of Co^{2+} from the mixture as solids while simultaneously increasing the purity of Li^{+} remaining in the solution, thereby enabling an efficient separation of Co^{2+} and Li^{+} ions.

Environmental Implications

This study pioneered the use of ferritin nanocages as efficient protein sorbents for the selective separation and recovery of critical metals from mixtures. Compared to other biosorption approaches such as LanM, ferritin leverages its unique property of concentrating adsorbed metal cations within its cavity, enabling integrated metal separation and recovery as high-grade solid salts through simple, environmentally friendly adsorption-precipitation processes under benign conditions. However, while AfFtn effectively separates Co^{2+}/Ni^{2+} from Li^{+}, it exhibits limited separation between Co^{2+} and Ni^{2+}. Future research should focus on engineering its open pores (e.g., altering the pore size, incorporating amino acids with metal-interacting side chains) to tune its affinity for different metals and achieve highly selective separation among diverse metal ions. Moreover, an in-depth evaluation of the ferritin-based recovery approach using realistic waste leachate is needed to develop a comprehensive understanding of its efficiency under practical conditions.

SUPPORTING INFORMATION

Detailed description of materials used and experimental methods, covering protein expression and purification, metal ion adsorption, Co^{2+} recovery through AfFtn-facilitated precipitation, protein concentration measurement, and SDS-PAGE, DLS, negative-stain TEM, and XRD analyses; relevant experimental results including purification and characterization of AfFtn nanocages (Figure S1A-C), additional negative-stain TEM images of purified AfFtn nanocages (Figure S2), calculated charge per protein (Figure S3A-C), and XRD analysis of precipitates formed in the Co^{2+}-Li+ mixture containing AfFtn nanocages and $NaHCO_3$ (Figure S4).

ACKNOWLEDGMENTS

This work was supported by the University of Pittsburgh Mascaro Center for Sustainable Innovation seeding grant, the Swanson School of Engineering-School of Public Health collaboration pilot award, and the Department of Civil and Environmental Engineering. We thank Dr. David Malehorn for assistance with ICP-OES.

CONFLICT OF INTEREST

The authors declare no competing financial interest.

REFERENCES

(1) Zhang, S.; Ding, Y.; Liu, B.; Chang, C. Supply and Demand of Some Critical Metals and Present Status of Their Recycling in WEEE. *Waste Management* **2017**, *65*, 113–127. https://doi.org/https://doi.org/10.1016/j.wasman.2017.04.003.

(2) Zeng, X.; Xiao, T.; Xu, G.; Albalghiti, E.; Shan, G.; Li, J. Comparing the Costs and Benefits of Virgin and Urban Mining. *Journal of Management Science and Engineering* **2022**, *7* (1), 98–106. https://doi.org/10.1016/j.jmse.2021.05.002.

(3) Haque, N.; Hughes, A.; Lim, S.; Vernon, C. Rare Earth Elements: Overview of Mining, Mineralogy, Uses, Sustainability and Environmental Impact. *Resources*. MDPI AG December 1, 2014, pp 614–635. https://doi.org/10.3390/resources3040614.

(4) Islam, A.; Swaraz, A. M.; Teo, S. H.; Taufiq-Yap, Y. H.; Vo, D. V. N.; Ibrahim, M. L.; Abdulkreem-Alsultan, G.; Rashid, U.; Awual, M. R. Advances in Physiochemical and Biotechnological Approaches for Sustainable Metal Recovery from E-Waste: A Critical Review. *Journal of Cleaner Production*. Elsevier Ltd November 10, 2021. https://doi.org/10.1016/j.jclepro.2021.129015.

(5) Zeng, X.; Mathews, J. A.; Li, J. Urban Mining of E-Waste Is Becoming More Cost-Effective Than Virgin Mining. *Environ Sci Technol* **2018**, *52* (8), 4835–4841. https://doi.org/10.1021/acs.est.7b04909.

(6) Cayumil, R.; Khanna, R.; Rajarao, R.; Mukherjee, P. S.; Sahajwalla, V. Concentration of Precious Metals during Their Recovery from Electronic Waste. *Waste Management* **2016**, *57*, 121–130. https://doi.org/https://doi.org/10.1016/j.wasman.2015.12.004.

(7) Chen, X.; Kang, D.; Cao, L.; Li, J.; Zhou, T.; Ma, H. Separation and Recovery of Valuable Metals from Spent Lithium Ion Batteries: Simultaneous Recovery of Li and Co in a Single Step. *Sep Purif Technol* **2019**, *210*, 690–697. https://doi.org/10.1016/j.seppur.2018.08.072.

(8) Wang, R.-C.; Lin, Y.-C.; Wu, S.-H. A Novel Recovery Process of Metal Values from the Cathode Active Materials of the Lithium-Ion Secondary Batteries. *Hydrometallurgy* **2009**, *99* (3), 194–201. https://doi.org/https://doi.org/10.1016/j.hydromet.2009.08.005.

(9) Cui, J.; Zhang, L. Metallurgical Recovery of Metals from Electronic Waste: A Review. *Journal of Hazardous Materials*. October 30, 2008, pp 228–256. https://doi.org/10.1016/j.jhazmat.2008.02.001.

(10) Kumar, M.; Nandi, M.; Pakshirajan, K. Recent Advances in Heavy Metal Recovery from Wastewater by Biogenic Sulfide Precipitation. *Journal of Environmental Management*. Academic Press January 15, 2021. https://doi.org/10.1016/j.jenvman.2020.111555.

(11) Patel, A.; Enman, J.; Gulkova, A.; Guntoro, P. I.; Dutkiewicz, A.; Ghorbani, Y.; Rova, U.; Christakopoulos, P.; Matsakas, L. Integrating Biometallurgical Recovery of Metals with Biogenic Synthesis of Nanoparticles. *Chemosphere* **2021**, *263*. https://doi.org/10.1016/j.chemosphere.2020.128306.

(12) Ilyas, S.; Lee, J. chun. Biometallurgical Recovery of Metals from Waste Electrical and Electronic Equipment: A Review. *ChemBioEng Reviews*. Wiley-Blackwell August 1, 2014, pp 148–169. https://doi.org/10.1002/cben.201400001.

(13) Zhuang, W. Q.; Fitts, J. P.; Ajo-Franklin, C. M.; Maes, S.; Alvarez-Cohen, L.; Hennebel, T. Recovery of Critical Metals Using Biometallurgy. *Current Opinion in Biotechnology*. Elsevier Ltd June 1, 2015, pp 327–335. https://doi.org/10.1016/j.copbio.2015.03.019.

(14) Cotruvo, J. A.; Featherston, E. R.; Mattocks, J. A.; Ho, J. V.; Laremore, T. N. Lanmodulin: A Highly Selective Lanthanide-Binding Protein from a Lanthanide-Utilizing Bacterium. *J Am Chem Soc* **2018**, *140* (44), 15056–15061. https://doi.org/10.1021/jacs.8b09842.

(15) Park, D. M.; Brewer, A.; Reed, D. W.; Lammers, L. N.; Jiao, Y. Recovery of Rare Earth Elements from Low-Grade Feedstock Leachates Using Engineered Bacteria. *Environ Sci Technol* **2017**, *51* (22), 13471–13480. https://doi.org/10.1021/acs.est.7b02414.

(16) Deblonde, G. J. P.; Mattocks, J. A.; Park, D. M.; Reed, D. W.; Cotruvo, J. A.; Jiao, Y. Selective and Efficient Biomacromolecular Extraction of Rare-Earth Elements Using Lanmodulin. *Inorg Chem* **2020**, *59* (17), 11855–11867. https://doi.org/10.1021/acs.inorgchem.0c01303.

(17) Jung, H.; Su, Z.; Inaba, Y.; West, A. C.; Banta, S. Genetic Modification of Acidithiobacillus Ferrooxidans for Rare-Earth Element Recovery under Acidic Conditions. *Environ Sci Technol* **2023**, *57* (48), 19902–19911. https://doi.org/10.1021/acs.est.3c05772.

(18) Ye, Q.; Jin, X.; Zhu, B.; Gao, H.; Wei, N. Lanmodulin-Functionalized Magnetic Nanoparticles as a Highly Selective Biosorbent for Recovery of Rare Earth Elements. *Environ Sci Technol* **2023**, *57* (10), 4276–4285. https://doi.org/10.1021/acs.est.2c08971.

(19) Sana, B.; Johnson, E.; Magueres, P. Le; Criswell, A.; Cascio, D.; Lim, S. The Role of Nonconserved Residues of Archaeoglobus Fulgidus Ferritin on Its Unique Structure and Biophysical Properties. *Journal of Biological Chemistry* **2013**, *288* (45), 32663–32672. https://doi.org/10.1074/jbc.M113.491191.

(20) He, D.; Marles-Wright, J. Ferritin Family Proteins and Their Use in Bionanotechnology. *New Biotechnology*. Elsevier December 25, 2015, pp 651–657. https://doi.org/10.1016/j.nbt.2014.12.006.

(21) Le Brun, N. E.; Crow, A.; Murphy, M. E. P.; Mauk, A. G.; Moore, G. R. Iron Core Mineralisation in Prokaryotic Ferritins. *Biochimica et Biophysica Acta - General Subjects*. August 2010, pp 732–744. https://doi.org/10.1016/j.bbagen.2010.04.002.

(22) Tetter, S.; Hilvert, D. Enzyme Encapsulation by a Ferritin Cage. *Angewandte Chemie* **2017**, *129* (47), 15129–15132. https://doi.org/10.1002/ange.201708530.

(23) Butts, C. A.; Swift, J.; Kang, S. G.; Di Costanzo, L.; Christiansen, D. W.; Saven, J. G.; Dmochowski, I. J. Directing Noble Metal Ion Chemistry within a Designed Ferritin Protein. *Biochemistry* **2008**, *47* (48), 12729–12739. https://doi.org/10.1021/bi8016735.

(24) Price, D. J.; Joshi, J. G. Ferritin. Binding of Beryllium and Other Divalent Metal Ions. *Journal of Biological Chemistry* **1983**, *258* (18), 10873–10880. https://doi.org/10.1016/s0021-9258(17)44357-2.

(25) Pead, S.; Durrant, E.; Webb, B.; Larsen, C.; Heaton, D.; Johnson, J.; Watt, G. D. *Metal Ion Binding to Apo, Holo, and Reconstituted Horse Spleen Ferritin*; 1995.

(26) Zheng, X.; Zhu, Z.; Lin, X.; Zhang, Y.; He, Y.; Cao, H.; Sun, Z. A Mini-Review on Metal Recycling from Spent Lithium Ion Batteries. *Engineering*. Elsevier Ltd June 1, 2018, pp 361–370. https://doi.org/10.1016/j.eng.2018.05.018.

(27) Sana, B.; Johnson, E.; Lim, S. The Unique Self-Assembly/Disassembly Property of Archaeoglobus Fulgidus Ferritin and Its Implications on Molecular Release from the Protein Cage. *Biochim Biophys Acta Gen Subj* **2015**, *1850* (12), 2544–2551. https://doi.org/10.1016/j.bbagen.2015.08.019.

(28) Jurrus, E.; Engel, D.; Star, K.; Monson, K.; Brandi, J.; Felberg, L. E.; Brookes, D. H.; Wilson, L.; Chen, J.; Liles, K.; Chun, M.; Li, P.; Gohara, D. W.; Dolinsky, T.; Konecny, R.; Koes, D. R.; Nielsen, J. E.; Head-Gordon, T.; Geng, W.; Krasny, R.; Wei, G. W.; Holst, M. J.; McCammon, J. A.; Baker, N. A. Improvements to the APBS Biomolecular Solvation Software Suite. *Protein Science* **2018**, *27* (1), 112–128. https://doi.org/10.1002/pro.3280.

(29) Pettersen, E. F.; Goddard, T. D.; Huang, C. C.; Meng, E. C.; Couch, G. S.; Croll, T. I.; Morris, J. H.; Ferrin, T. E. UCSF ChimeraX: Structure Visualization for Researchers, Educators, and Developers. *Protein Science* **2021**, *30* (1), 70–82. https://doi.org/10.1002/pro.3943.

(30) Goddard, T. D.; Huang, C. C.; Meng, E. C.; Pettersen, E. F.; Couch, G. S.; Morris, J. H.; Ferrin, T. E. UCSF ChimeraX: Meeting Modern Challenges in Visualization and Analysis. *Protein Science* **2018**, *27* (1), 14–25. https://doi.org/10.1002/pro.3235.

(31) Meng, E. C.; Goddard, T. D.; Pettersen, E. F.; Couch, G. S.; Pearson, Z. J.; Morris, J. H.; Ferrin, T. E. UCSF ChimeraX: Tools for Structure Building and Analysis. *Protein Science* **2023**, *32* (11). https://doi.org/10.1002/pro.4792.

(32) Zhou, H. X.; Pang, X. Electrostatic Interactions in Protein Structure, Folding, Binding, and Condensation. *Chemical Reviews*. American Chemical Society February 28, 2018, pp 1691–1741. https://doi.org/10.1021/acs.chemrev.7b00305.

(33) Sheinerman, F. B.; Honig, B. On the Role of Electrostatic Interactions in the Design of Protein-Protein Interfaces. *J Mol Biol* **2002**, *318* (1), 161–177. https://doi.org/10.1016/S0022-2836(02)00030-X.

Supporting Information

Ferritin Protein Nanocages for Selective Separation and Recovery of Critical Metals

Zhiqian Han[a], Yifei Ma[a], Meng Wang[a,*]

[a]Department of Civil and Environmental Engineering, University of Pittsburgh, 3700 O'Hara St., Pittsburgh, PA 15261

*Address correspondence to meng.wang@pitt.edu, 412-624-9207

List of Supporting Texts

List of Supporting Figures

Text S1. Materials

Ampicillin sodium salt, HisPurTM Ni-NTA Resin, Cobalt(II) chloride hexahydrate (98%-102%), Nickel(II) chloride hexahydrate (99.95%), lysozyme, and Lithium chloride, ultra dry, 99.9% (metals basis) were obtained from Thermo Scientific (Thermo Scientific, Waltham, MA). Ammonium Sulfate, Isopropyl-β-D-thiogalactopyranoside (IPTG) (Dioxane-free), Tris Hydrochloride, Sodium Chloride, Sodium Bicarbonate Certified A.C.S., Bovine Serum Albumin (BSA) Microbiological Grade Powder, and Nitric acid trance metal grade were obtained from Fisher Scientific (Fisher, Waltham, MA). SIGMAFASTTM Protease Inhibitor Cocktail Tablets, EDTA-Free was obtained from Sigma-Aldrich (Sigma-Aldrich, St. Louis, MO). PD-10 columns were from Cytiva (Cytiva, Marlborough, MA). Micro Bio-Spin® Columns with Bio-Gel® P-6 (Bio-Rad, Hercules, CA). DI water was obtained from the Millipore Synergy-R system (MilliporeSigma, St. Louis, MO).

Text S2. Protein Expression and Purification

Protein Expression. The coding sequence of *Archaeoglobus fulgidus* ferritin (AfFtn) was obtained from GenScript (GenScript, Piscataway, NJ) and transformed into BL-21(DE3) Competent *Escherichia coli* (New England Biolabs, Ipswich, MA) via heat shock following the suppler's transformation protocol. Single colonies were selected from LB agar plates containing 50 μg/mL ampicillin and inoculated in 10 mL LB medium (100 μg/mL ampicillin), then cultured overnight at 37°C with shaking at 250 rpm (round per minute). The overnight cultures were diluted 1:100 in 200 mL fresh LB medium and grown at 37 °C, shaking at 250 rpm for 2-2.5 hours until the OD_{600} reached 0.6-0.8. Cultures were then chilled on ice, induced with 500 μM isopropyl-β-D-thiogalactopyranoside (IPTG), and incubated overnight at 20°C. Afterward, cells were collected by centrifugation at 20,000 × g for two minutes at room temperature, and the resulting pellets were frozen at -80°C until use.

Protein Purification. The purification of AfFtn nanocages was performed following a previously reported protocol with modifications.[1] Briefly, the collected *E. coli* cells were resuspended in 10 mL of pH 8.0 50 mM Tris-HCl buffer containing 600 mM NaCl and protease inhibitor and sonicated on the ice using a Branson Sonifier 550 in pulse mode (10% intensity), with 50 ms on and 50 ms off intervals. Each 30-second sonication was followed by a 30-second pause until the solution became clear. The insoluble fraction was then removed by centrifugation at 12,000 × g, 4 °C for 20 minutes. The supernatant containing soluble AfFtn was heated to 70°C for 20 minutes, followed by a second centrifuged at 12,000 × g, 4 °C for 20 minutes. The resulting supernatant was treated with ammonium sulfate to a final concentration of 70% saturation at 0 °C to precipitate AfFtn, which was then resuspended in pH 8.0 50 mM Tris-HCl with 600 mM NaCl. Any residual ammonium sulfate in the resuspended AfFtn solution was removed using PD-10 desalting columns. Assembled AfFtn nanocages and other proteins in the eluate were then separated on an NGC™ Chromatography System (Bio-Rad, Hercules, CA) with a HiPrep 16/60 Sephacryl S-400HR column (Cytiva, Marlborough, MA). The purified AfFtn nanocages were collected at the corresponding FPLC peak, concentrated using Vivaspin® 15R Centrifugal concentrators with a 5000 molecular weight

cutoff (MWCO) membrane (Sartorius, Germany), analyzed by Sodium dodecyl-sulfate polyacrylamide gel electrophoresis (SDS-PAGE), and stored at 4 °C until use.

Text S3. Metal Ion Adsorption by AfFtn Nanocages

Adsorption experiments were conducted in 1.5 mL microcentrifuge tubes on a Standard Analog Shaker (VWR, USA) at 60 rpm and room temperature. For assessing adsorption capability, 50 - 200 μg/mL of purified AfFtn nanocages was mixed with 0.25 mM Co^{2+} in 200 μL of Tris-NaCl buffer (50 mM Tris-HCl, 300 mM NaCl, pH 8.0) and incubated overnight. BSA and lysozyme were also evaluated under identical conditions as controls. After incubation, 60 μL of the adsorption reaction solution was passed through a micro bio-spin P-6 gel desalting column with a molecular weight cut-off of 6 kDa (Bio-Rad, Hercules, CA) to remove unbound, free metal ions. The eluate containing protein-adsorbed metal ions was diluted with DI water containing 1% nitric acid to create a 1500 μL sample solution for metal ion analysis by inductively coupled plasma-optical emission spectrometry (Agilent 5000 ICP-OES, Agilent, Santa Clara, CA). Absorbance wavelengths were set to 234.892 nm for Co^{2+}, 231.604 nm for Ni^{2+}, and 670.783 nm for Li^{+}.

To evaluate the adsorption isotherm, 100 μg/mL AfFtn nanocages were incubated overnight with varying concentrations of individual metal ions (Co^{2+}, Ni^{2+}, or Li^{+}) in 200 μL of Tris-NaCl buffer (50 mM Tris-HCl, 300 mM NaCl, pH 8.0). Kinetic experiments were conducted by mixing 100 μg/mL AfFtn with 0.5 mM Co^{2+} or Ni^{2+} in a 2 mL Tris-NaCl buffer, with samples taken at intervals from 0 to 2 hours. At each time point, 65 μL of the reaction solution was passed through to P-6 gel columns to immediately remove unbound metal ions.

For selective separation and recovery experiments, combinations of two metal ions (Co^{2+}, Ni^{2+}, or Li^{+}) were introduced into the reaction solution. After adsorption and desalting, the concentrations of each AfFtn adsorbed metal ion in the eluate were measured using ICP-OES.

The average local concentration of adsorbed metal ions within the AfFtn cavity (C_f) was estimated using the following equation, assuming a uniform distribution of all adsorbed metal ions within the cavity of the AfFtn nanocages:

$$C_f = \frac{mol_{Adsorbed\ metal\ ion}}{V_{AfFtn}} = \frac{V_{ICP-OES} \times C_{ICP-OES}}{\frac{m_{AfFtn}}{24 \times M_{AfFtn\ monomer}} \times N_A \times V_{mAfFtn}}$$

Where $mol_{Adsorbed\ metal\ ion}$ is the molar quantity of AfFtn-adsorbed metal ions (mol); V_{AfFtn} is the total internal volume of AfFtn nanocages in the adsorption reaction solution (L); $V_{ICP\text{-}OES}$ is the sample volume prepared for ICP-OES analysis (L); $C_{ICP\text{-}OES}$ is the metal ion concentration measured by ICP-OES (M); m_{AfFtn} is the mass of AfFtn in the reaction solution (g), calculated as the volume of reaction solution multiplied by AfFtn's final mass concentration (100 μg/mL); M_{AfFtn} is the molecular weight of AfFtn nanocage, calculated as 24 × $M_{AfFtn\ monomer}$. 24 is number of AfFtn monomer per assembled AfFtn nanocage, and $M_{AfFtn\ monomer}$ is the molecular weight of a single AfFtn monomer (20.51 kDa); N_A is the Avogadro constant (6.022 × 10^{23} mol^{-1}); V_{mAfFtn} is the internal volume of a single AfFtn nanocage (L), assuming AfFtn to be a spherical structure with an 8 nm inner diameter.[1]

The average number of metal ions adsorbed by each AfFtn nanocage ($N_{metal\ ion}$) was calculated using the following equation:

$$N_{metal\ ion} = C_f \times V_{mAfFtn} \times N_A$$

Where C_f is the average local concentration of adsorbed metal ions within the AfFtn cavity (M); V_{mAfFtn} is the internal volume of a single AfFtn nanocage (L); and N_A is the Avogadro constant (6.022 × 10^{23} mol^{-1}).

Text S4. Co^{2+} Recovery through Precipitation

The selective precipitation of Co^{2+} facilitated by AfFtn was assessed in 1.5 mL microcentrifuge tubes on a Standard Analog Shaker (VWR, USA) at 60 rpm and room temperature, using sodium bicarbonate as the carbonate source. For each test, 100 μg/mL AfFtn, 66.7 mM $NaHCO_3$, and 8 mM metal ions (Co^{2+} and Li^+) were mixed in 300 μL of Tris-NaCl buffer (50 mM Tris-HCl, 300 mM NaCl, pH 8.0) and incubated for varying time (0 - 5 days). Two control groups were included: one without AfFtn and another without both AfFtn and $NaHCO_3$. After each incubation period, the solutions were centrifuged at 20,000 × g for 2 minutes, and the supernatants were carefully removed. The resulting pellets were resuspended in DI water to the original volume, diluted into 1.2 mL of 1% nitric acid, and analyzed for Co^{2+} and Li^+ concentrations using ICP-OES.

Text S5. Protein Concentration Measurement

Protein concentration was measured using the Pierce™ BCA Protein Assay Kit (Thermo Scientific). A protein ladder was prepared by diluting a BSA standard solution. To create the working reagent, reagents A and B were combined in a 50:1 ratio. For the assay, 25 µL of each protein ladder and sample was added to a 96-well plate, followed by 200 µL of the working reagent. The plate was incubated at 37°C for 30 minutes, and absorbance was measured at 562 nm using a BioTek Synergy HTX Multimode Reader (Agilent, CA) to quantify protein concentrations.

Text S6. SDS-PAGE Analysis

The 4× SDS-PAGE sample loading buffer was prepared by mixing 4× Laemmli sample buffer Bio-Rad, Hercules, CA) with 2-mercaptoethanol at a volume ratio of 9:1. This loading buffer was then combined with protein samples at a 1:3 volume ratio and heated at 95 °C for 5 minutes. The samples were subsequently loaded onto Any kD Mini-PROTEAN TGX Stain-free precast protein gels (Bio-Rad, Hercules, CA) for fractionation and visualized using Azure 300 imaging system (Azure Biosystems, Dublin, CA). Precision Plus Protein™ All Blue Standard (Bio-Rad, Hercules, CA) was used as the molecular weight ladder for SDS-PAGE analysis.

Text S7. Dynamic light scattering (DLS)

Sizing and polydispersity measurements of AfFtn nanocages were performed using a Beckman Coulter Particle Size Analyzer at room temperature. The purified AaLS-13 nanocages were diluted to a protein concentration of 500 μg/mL in a pH 8.0 50 mM Tris-HCl buffer containing 300 mM NaCl, passed through a 0.22 μm low protein retention syringe filter, and immediately subjected to DLS analysis.

Text S8. Negative-Stain Transmission Electron Microscopy (TEM)

Purified AfFtn nanocages were diluted to a concentration of 200 μg/mL in a 50 mM Tris-HCl buffer (pH 8.0, with 300 mM NaCl) and applied onto copper grids (200 mesh, pure carbon film without Formvar, PELCO). After a 2-minute incubation, excess AfFtn solution was wicked away using filter paper, and the grid was rinsed in 0.22 μm-filtered DI water for 1 minute before wicking with filter paper. This rinsing step was repeated three times to ensure proper cleaning. Subsequently, 20 μL of 2% uranyl acetate solution was applied onto the grid and incubated for 2 minutes to stain AfFtn nanocages. After removing the excess stain solution with filter paper, the grid was air-dried and stored at room temperature prior to imaging. TEM images were acquired using a Hitachi H9500 transmission electron microscope operated at 200 kV at the Nanoscale Fabrication and Characterization Facility (NFCF) at the University of Pittsburgh (Pitt).

Text S9. X-Ray Diffraction (XRD)

The pellet formed by incubating Co^{2+}, Li^{+}, and HCO_3^{-} with AfFtn was collected and dried in a desiccator at room temperature. XRD data were acquired using a Bruker X-ray Diffraction System at the Nanoscale NFCF at Pitt. Scans were performed over a 2θ range of 10° to 95°, and the collected diffraction patterns were analyzed using DIFFRAC.EVA to identify peaks and compare with reference diffraction data.

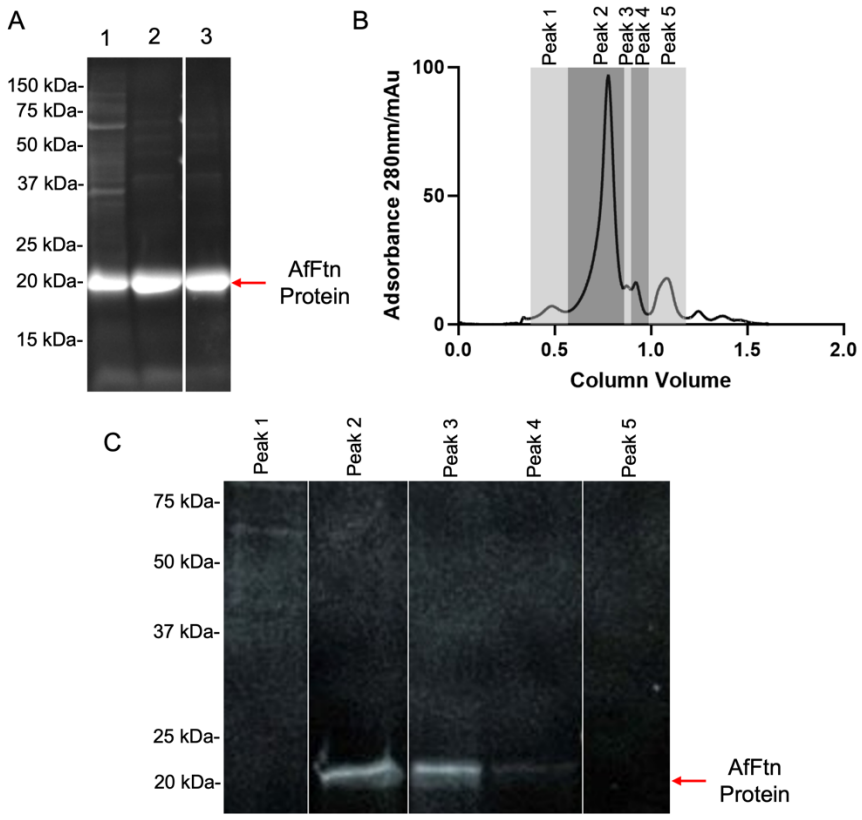

149

150 **Figure S1.** Purification of AfFtn nanocages. (A) SDS-PAGE analysis of AfFtn samples prior to size-
151 exclusion chromatography (SEC) purification. Lane 1: Clear lysate (supernatant obtained after
152 centrifugation of the crude lysate); Lane 2: Supernatant following heating of the clear lysate at 70 °C for
153 20 minutes and subsequent centrifugation; Lane 3: Resuspended pellet from the supernatant treated with
154 ammonium sulfate at 70% saturation. (B) SEC elution profile of ammonium sulfate-precipitated AfFtn
155 samples. Five peaks were identified and collected for SDS-PAGE analysis, and Peak 2 at 0.8 column volume
156 corresponds to the assembled, intact AfFtn nanocages. (C) SDS-PAGE analysis of different SEC peaks.

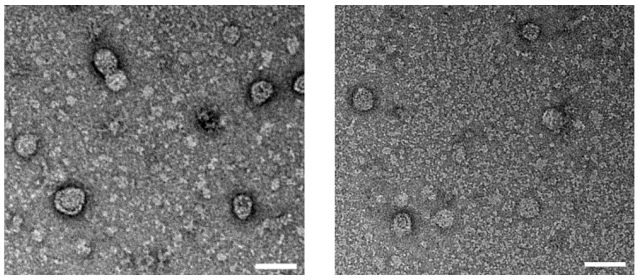

Figure S2. Additional negative-stain TEM images of purified AfFtn nanocages, which exhibit spherical morphologies with "dark" stained edges. Scale bar: 50 nm.

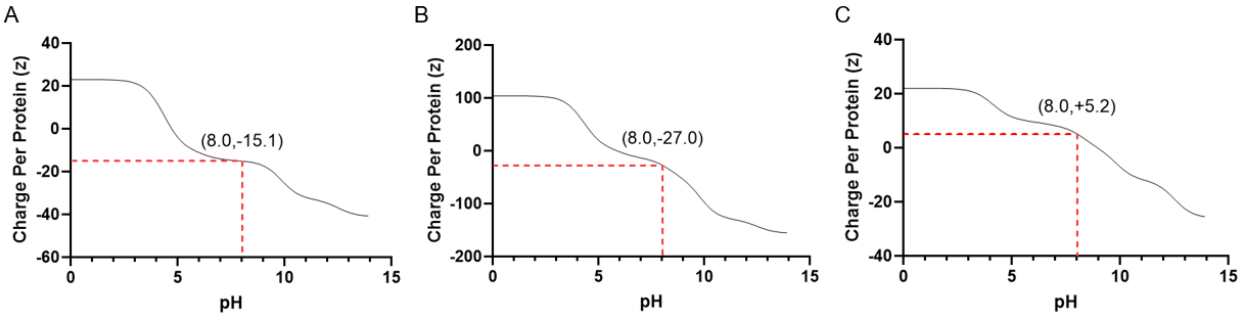

Figure S3. Calculated charge per protein for AfFtn monomer (A), BSA (B), and lysozyme (C) as a function of pH.

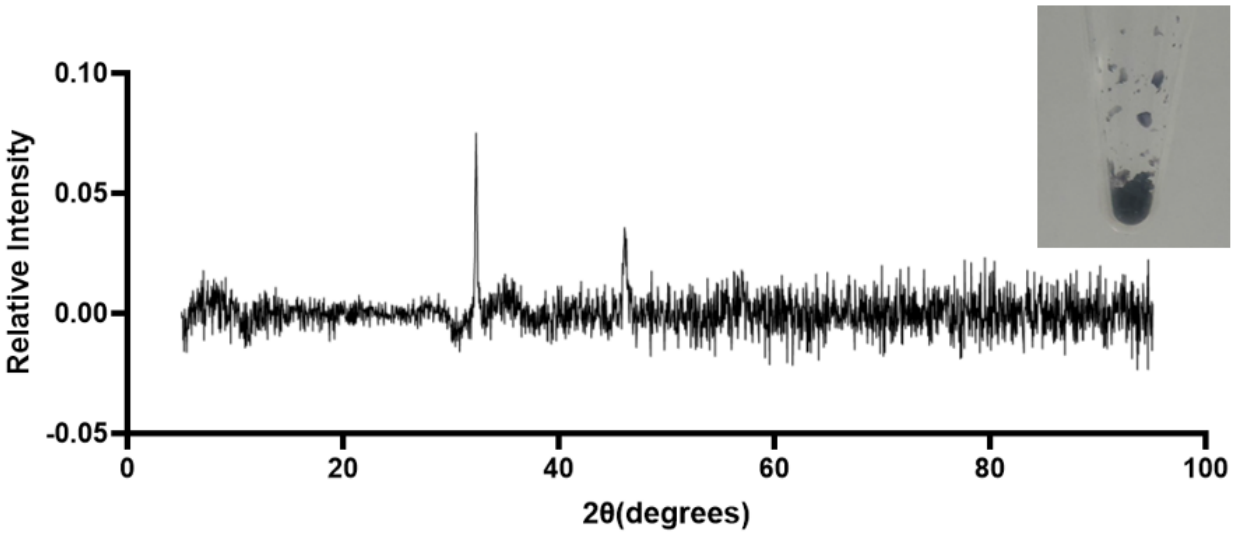

163

164 **Figure S4.** XRD analysis of precipitates formed in the Co^{2+}-Li+ mixture containing AfFtn nanocages and
165 $NaHCO_3$. Distinct peaks were observed around 2θ values of 32° and 46°, closely aligning with the
166 characteristic XRD pattern of cobalt carbonate. The prepared XRD sample, displayed in the upper right
167 insert, exhibits a dark purple-black crystal.

Reference

(1) Tetter, S.; Hilvert, D. Enzyme Encapsulation by a Ferritin Cage. *Angewandte Chemie* **2017**, *129* (47), 15129–15132. https://doi.org/10.1002/ange.201708530.